



# CHORUS

This is the accepted manuscript made available via CHORUS. The article has been published as:

## Differential Cross Section and Photon-Beam Asymmetry for the $\gamma \rightarrow p \rightarrow \pi^{-} \Delta^{++}(1232)$ Reaction at Forward $\pi^{-}$ Angles for $E_{\gamma}=1.5-2.95$ GeV

H. Kohri *et al.* (LEPS Collaboration)

Phys. Rev. Lett. **120**, 202004 — Published 18 May 2018

DOI: [10.1103/PhysRevLett.120.202004](https://doi.org/10.1103/PhysRevLett.120.202004)

1 **Differential cross section and photon-beam asymmetry for the  $\vec{\gamma}p$**   
2  **$\rightarrow \pi^- \Delta^{++}(\mathbf{1232})$  reaction at forward  $\pi^-$  angles for  $E_\gamma=1.5-2.95$**   
3 **GeV**

4 H. Kohri,<sup>1,2</sup> S. H. Shiu,<sup>2,3</sup> W. C. Chang,<sup>2</sup> Y. Yanai,<sup>1</sup> D. S. Ahn,<sup>4</sup> J. K. Ahn,<sup>5</sup>  
5 J. Y. Chen,<sup>6</sup> S. Daté,<sup>7</sup> H. Ejiri,<sup>1</sup> H. Fujimura,<sup>8</sup> M. Fujiwara,<sup>1,9</sup> S. Fukui,<sup>1</sup> W. Gohn,<sup>10</sup>  
6 K. Hicks,<sup>11</sup> A. Hosaka,<sup>1</sup> T. Hotta,<sup>1</sup> S. H. Hwang,<sup>12</sup> K. Imai,<sup>13</sup> T. Ishikawa,<sup>14</sup> K. Joo,<sup>10</sup>  
7 Y. Kato,<sup>15</sup> Y. Kon,<sup>1</sup> H. S. Lee,<sup>16</sup> Y. Maeda,<sup>17</sup> T. Mibe,<sup>18</sup> M. Miyabe,<sup>14</sup> Y. Morino,<sup>18</sup>  
8 N. Muramatsu,<sup>14</sup> T. Nakano,<sup>1</sup> Y. Nakatsugawa,<sup>18,19</sup> S. i. Nam,<sup>20</sup> M. Niiyama,<sup>21</sup>  
9 H. Noumi,<sup>1</sup> Y. Ohashi,<sup>7</sup> T. Ohta,<sup>1,22</sup> M. Oka,<sup>1</sup> J. D. Parker,<sup>21,23</sup> C. Rangacharyulu,<sup>24</sup>  
10 S. Y. Ryu,<sup>1</sup> T. Sawada,<sup>2,25</sup> H. Shimizu,<sup>14</sup> E. A. Stokovsky,<sup>26,1</sup> Y. Sugaya,<sup>1</sup>  
11 M. Sumihama,<sup>27</sup> T. Tsunemi,<sup>21</sup> M. Uchida,<sup>28</sup> M. Ungaro,<sup>10</sup> S. Y. Wang,<sup>2,29</sup> and M. Yosoi<sup>1</sup>

12 (LEPS Collaboration)

13 <sup>1</sup>*Research Center for Nuclear Physics, Osaka University, Ibaraki, Osaka 567-0047, Japan*

14 <sup>2</sup>*Institute of Physics, Academia Sinica, Taipei 11529, Taiwan*

15 <sup>3</sup>*Department of Physics, National Central University, Taoyuan City 32001, Taiwan*

16 <sup>4</sup>*RIKEN Nishina Center, 2-1 Hirosawa, Wako, Saitama 351-0198, Japan*

17 <sup>5</sup>*Department of Physics, Korea University, Seoul 02841, Republic of Korea*

18 <sup>6</sup>*Light Source Division, National Synchrotron*

19 *Radiation Research Center, Hsinchu, 30076, Taiwan*

20 <sup>7</sup>*Japan Synchrotron Radiation Research Institute, Sayo, Hyogo 679-5143, Japan*

21 <sup>8</sup>*Wakayama Medical College, Wakayama, 641-8509, Japan*

22 <sup>9</sup>*National Institutes for Quantum and Radiological*

23 *Science and Technology, Tokai, Ibaraki 319-1195, Japan*

24 <sup>10</sup>*Department of Physics, University of Connecticut, Storrs, CT 06269-3046, USA*

25 <sup>11</sup>*Department of Physics and Astronomy, Ohio University, Athens, Ohio 45701, USA*

26 <sup>12</sup>*Korea Research Institute of Standards and*

27 *Science (KRISS), Daejeon 34113, Republic of Korea*

28 <sup>13</sup>*Advanced Science Research Center, Japan Atomic*

29 *Energy Agency, Tokai, Ibaraki 319-1195, Japan*

30  
31  
32  
33  
34  
35  
36  
37  
38  
39  
40  
41  
42  
43  
44  
45  
46  
47  
48  
49  
50

<sup>14</sup>*Research Center for Electron Photon Science,*

*Tohoku University, Sendai, Miyagi 982-0826, Japan*

<sup>15</sup>*Kobayashi-Maskawa Institute, Nagoya University, Nagoya, Aichi 464-8602, Japan*

<sup>16</sup>*Rare Isotope Science Project, Institute for Basic Science, Daejeon 34047, Korea*

<sup>17</sup>*Proton Therapy Center, Fukui Prefectural Hospital, Fukui 910-8526, Japan*

<sup>18</sup>*High Energy Accelerator Organization (KEK), Tsukuba, Ibaraki 305-0801, Japan*

<sup>19</sup>*Institute of High Energy Physics, Chinese Academy of Sciences, Beijing 100049, China*

<sup>20</sup>*Department of Physics, Pukyong National University*

*(PKNU), Busan 608-737, Republic of Korea*

<sup>21</sup>*Department of Physics, Kyoto University, Kyoto 606-8502, Japan*

<sup>22</sup>*Department of Radiology, The University of Tokyo Hospital, Tokyo 113-8655, Japan*

<sup>23</sup>*Neutron Science and Technology Center, Comprehensive Research  
Organization for Science and Society (CROSS), Tokai, Ibaraki 319-1106, Japan*

<sup>24</sup>*Department of Physics and Engineering Physics, University*

*of Saskatchewan, Saskatoon, SK S7N 5E2, Canada*

<sup>25</sup>*Physics Department, University of Michigan, Michigan 48109-1040, USA*

<sup>26</sup>*Joint Institute for Nuclear Research, Dubna, Moscow Region, 142281, Russia*

<sup>27</sup>*Department of Education, Gifu University, Gifu 501-1193, Japan*

<sup>28</sup>*Department of Physics, Tokyo Institute of Technology, Tokyo 152-8551, Japan*

<sup>29</sup>*ChemMatCARS, The University of Chicago, Argonne, Illinois 60439, USA*

(Dated: March 12, 2018)

## Abstract

51

52 Differential cross sections and photon-beam asymmetries for the  $\vec{\gamma}p \rightarrow \pi^- \Delta^{++}(1232)$  reaction  
53 have been measured for  $0.7 < \cos \theta_{\pi}^{c.m.} < 1$  and  $E_{\gamma}=1.5-2.95$  GeV at SPring-8/LEPS. The first-  
54 ever high statistics cross-section data are obtained in this kinematical region, and the asymmetry  
55 data for  $1.5 < E_{\gamma}(\text{GeV}) < 2.8$  are obtained for the first time. This reaction has a unique feature for  
56 studying the production mechanisms of a pure  $u\bar{u}$  quark pair in the final state from the proton.  
57 Although there is no distinct peak structure in the cross sections, a non-negligible excess over the  
58 theoretical predictions is observed at  $E_{\gamma}=1.5-1.8$  GeV. The asymmetries are found to be negative in  
59 most of the present kinematical regions, suggesting the dominance of  $\pi$  exchange in the  $t$  channel.  
60 The negative asymmetries at forward meson production angles are different from the asymmetries  
61 previously measured for the photoproduction reactions producing a  $d\bar{d}$  or an  $s\bar{s}$  quark pair in the  
62 final state. Advanced theoretical models introducing nucleon resonances and additional unnatural-  
63 parity exchanges are needed to reproduce the present data.

64 PACS numbers: 13.60.Le,14.20Gk,14.40Be,14.70.Bh,25.20Lj

65 The photoproduction of a  $d\bar{d}$  quark pair and an  $s\bar{s}$  quark pair in the final state has been  
66 extensively studied by the  $\gamma p \rightarrow \pi^+ n$  [1–3] and  $\gamma p \rightarrow K^+ \Lambda$  and  $K^+ \Sigma^0$  [4–11] reactions,  
67 respectively. However, the production of a  $u\bar{u}$  quark pair in the final state has not been  
68 well studied. Although the production of a  $\pi^0$  meson, with a quark-model wavefunction of  
69  $(u\bar{u} - d\bar{d})/\sqrt{2}$ , or  $\eta$  meson, with a wavefunction of  $(u\bar{u} + d\bar{d} + s\bar{s})/\sqrt{3}$ , includes the  $u\bar{u}$  quark-  
70 pair production, an exclusive study of a pure  $u\bar{u}$  quark-pair production is desired. The  $\gamma p$   
71  $\rightarrow \pi^- \Delta^{++}$  reaction is a unique channel to study the photoproduction mechanism of a pure  
72  $u\bar{u}$  quark pair in the final state from the proton.

73 In quark models, there exist more nucleon resonances than those experimentally observed  
74 so far [12]. Since nucleon resonances have relatively wide widths and are overlapping each  
75 other, rich physics observables with a wide angular and energy range are needed to study  
76 new resonances. The differential cross sections for the  $\gamma p \rightarrow \pi^- \Delta^{++}$  reaction were measured  
77 by SLAC at the higher energies of  $E_\gamma=4, 5, 8, 11,$  and  $16$  GeV [13–15]. At medium energies,  
78 there are only scarce existing data taken by SLAC at  $2.8$  GeV [16], by CEA for  $E_\gamma=0.5-1.8$   
79 GeV [17], by LAMP2 for  $E_\gamma=2.4-4.8$  GeV [18], by DESY for  $E_\gamma=0.3-5.8$  GeV [19], and by  
80 SAPHIR for  $E_\gamma=1.1-2.6$  GeV [20]. Although the  $\pi^- \Delta^{++}$  final state is one of prospective  
81 channels to study new nucleon resonances [12], cross-section data with a wide angular and  
82 energy range are missing in the world data set.

83 Basically, the photon-beam asymmetries are  $+1$  for  $\rho$  exchange and are  $-1$  for  $\pi$  exchange  
84 in the  $t$  channel in the case of the  $\vec{\gamma} p \rightarrow \pi^- \Delta^{++}$  reaction, which is the same as the case of the  
85  $\vec{\gamma} p \rightarrow \pi^+ n$  reaction [21]. There were three asymmetry measurements at the forward  $\pi^-$  angles  
86 of  $|t| < 0.5$  GeV<sup>2</sup> ( $0.8 < \cos \theta_\pi^{c.m.}$ ) at  $2.8$  GeV,  $4.7$  GeV, and  $16$  GeV by SLAC [16, 22], where  
87  $t$  is the Mandelstam variable defined by  $t=(p_\pi - p_\gamma)^2$ . Although negative asymmetries are  
88 suggested by these measurements, the number of the data points is limited and the data have  
89 large statistical uncertainties. In contrast, pseudoscalar meson photoproduction of either a  
90  $\pi^+$  or a  $K^+$  has positive asymmetries at the forward meson angles of  $0.6 < \cos \theta_{\pi,K}^{c.m.} < 1$  when  
91 the total energy  $W$  is higher than the third nucleon resonance region  $W \sim 1.7$  GeV ( $E_\gamma \sim 1.1$   
92 GeV) [1, 3–8]. The  $\pi^-$  photoproduction data may well have a different reaction mechanism  
93 than that of other pseudoscalar mesons. Combining the  $\pi^- \Delta^{++}$  data with the established  
94  $\pi^+$  and  $K^+$  photoproduction data is helpful to achieve a unified understanding of hadron  
95 photoproduction.

96 In this Letter, we present the first-ever high statistics differential cross-section and

97 photon-beam asymmetry data for the  $\vec{\gamma}p \rightarrow \pi^- \Delta^{++}$  reaction at the forward  $\pi^-$  angles of  
 98  $0.7 < \cos \theta_{\pi}^{c.m.} < 1$ . The data obtained over the energy range of  $E_{\gamma}=1.5$ -2.95 GeV, covering  
 99 most of the nucleon resonance region, enabled us to study both nucleon resonances and  
 100 hadron photoproduction dynamics.

101 The experiment was carried out using the LEPS beam line [23] at the SPring-8 facility  
 102 in Japan. The photon beam was produced by the laser backscattering technique using a  
 103 deep-UV laser with a wavelength of 257 nm [24]. The energy range of tagged photons was  
 104 from 1.5 to 2.96 GeV. The laser light was polarized linearly with a polarization degree of  
 105 98%. The polarization of tagged photons was 88% at 2.96 GeV and was 28% at 1.5 GeV  
 106 [25]. The photon beam was incident on a liquid hydrogen target (LH<sub>2</sub>) with a length of 16  
 107 cm.

108 Charged particles emitted from the LH<sub>2</sub> target were detected at forward angles by us-  
 109 ing the LEPS spectrometer. The aerogel Cherenkov counter was not used, and electrons  
 110 or positrons were vetoed using a plastic scintillation counter installed at the downstream  
 111 position of the three drift chambers. For the details about the LEPS spectrometer, see  
 112 Refs. [4, 23, 25].

113 Events with a  $\pi^-$  meson were identified from its mass within  $3\sigma$  where  $\sigma$  is the momentum  
 114 dependent mass resolution and was measured to be 60 and 110 MeV/ $c^2$  for 1 and 2 GeV/ $c$   
 115 momentum pions, respectively. The events from the LH<sub>2</sub> target were selected by a cut on  
 116 the  $z$ -vertex distribution. Contamination events from the start counter, placed downstream  
 117 of the target, were 0.5% at most.

118 Figure 1 shows the missing-mass spectra for the  $\gamma p \rightarrow \pi^- X$  reaction. The  $\Delta^{++}(1232)$   
 119 peaks are clearly observed at 1.23 GeV/ $c^2$ . The contribution from electrons, mainly orig-  
 120 inating from the  $e^+e^-$  pair creation, is observed for  $0.966 < \cos \theta_{\pi}^{c.m.} < 1$ . The number of  
 121  $\pi^- \Delta^{++}$  events was about 400 k in total.

122 The  $\gamma p \rightarrow \pi^- \Delta^{++}$  reaction events were selected by fitting a missing-mass spectrum with  
 123 curves for the  $\Delta^{++}$  peak,  $\rho$ ,  $2\pi$ ,  $3\pi$  productions, and electron background based on GEANT  
 124 simulations. For the  $\rho$ -meson productions, the differential cross sections and decay angular  
 125 distributions in Ref. [20] were assumed, and the multi-pion productions according to Lorentz-  
 126 invariant Fermi phase space were performed for the  $2\pi$  and  $3\pi$  productions. The electron  
 127 background events were generated to reproduce the momentum distributions of the real data.  
 128 The number of adjustable parameters in the fit was 5 in total. No interference between the

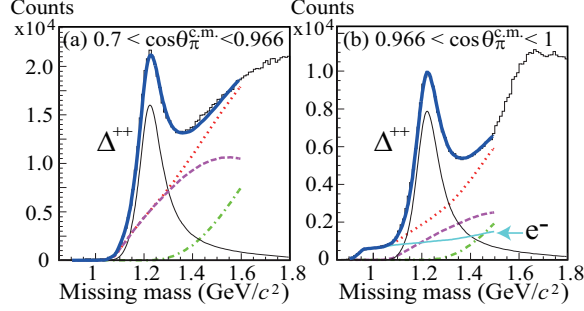


FIG. 1. Missing-mass spectra for the  $\gamma p \rightarrow \pi^- X$  reaction for  $E_\gamma=1.5-2.95$  GeV. The thick solid curves (blue) are the results of the fits, and the thin solid curves (black) are the  $\Delta^{++}$  contributions. The dotted curves (red) are the total contribution from backgrounds. The dashed (purple) and dotted-dashed (green) curves are the contributions from  $\rho/2\pi$  and  $3\pi$  productions, respectively. The curve (light blue) indicated by the arrow is the contribution from the electron background.

129  $\pi^- \Delta^{++}$  and other reactions was assumed in this analysis using single  $\pi^-$  events. The shape of  
 130 the  $\Delta^{++}(1232)$  was assumed to be given by a Jackson relativistic Breit-Wigner form [14, 26],

$$B(m) \propto \frac{m_0 \Gamma(m)}{(m^2 - m_0^2)^2 + m_0^2 \Gamma^2(m)}, \quad (1)$$

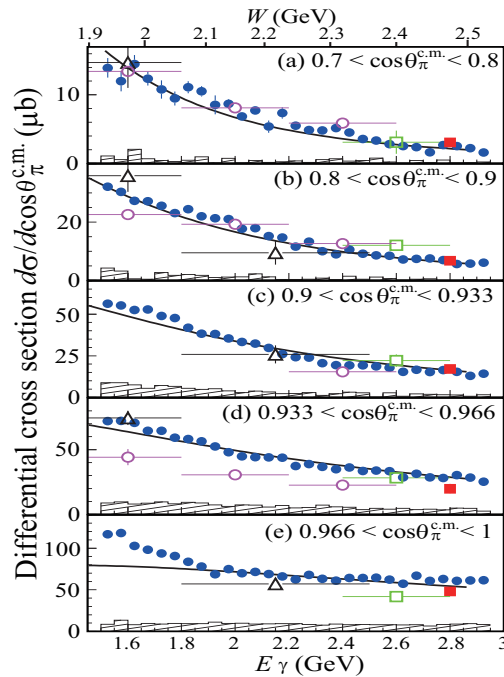
131 with

$$\Gamma(m) = \Gamma(m_0) \left(\frac{q}{q_0}\right)^3 \left(\frac{am_\pi^2 + q_0^2}{am_\pi^2 + q^2}\right) \left(\frac{m_0}{m}\right), \quad (2)$$

132 where  $m_0 = 1.232$  GeV,  $\Gamma(m_0) = 0.117$  GeV,  $a = 2.2$ , with  $q(q_0)$  being the c.m.-system  
 133 momentum at masses  $m(m_0)$  in the  $\Delta^{++}$  rest system. As a result of the fit, the  $\Delta^{++}$  yield for  
 134 the relativistic Breit-Wigner form (including the tail) was obtained for each incident photon  
 135 energy and angular bin. The acceptance of the LEPS spectrometer for  $\pi^-$  mesons was  
 136 obtained by the GEANT simulations. The differential cross sections for the  $\pi^- \Delta^{++}$  reaction  
 137 were obtained by using the same method described in Ref. [4]. The LEPS spectrometer has  
 138 almost the same acceptance for the  $\pi^-$  and  $\pi^+$  mesons, and the cross sections for the  $\gamma p$   
 139  $\rightarrow \pi^+ n$  reaction [1] obtained from the same data set agree well with the data obtained by  
 140 CLAS [2] and DESY [27].

141 Figure 2 shows the differential cross sections for the  $\gamma p \rightarrow \pi^- \Delta^{++}$  reaction as a func-  
 142 tion of  $E_\gamma$ . The cross sections decrease rapidly with increasing photon energy for  $0.7 <$   
 143  $\cos \theta_\pi^{c.m.} < 0.933$ . The energy dependence of the cross sections is small for  $0.966 < \cos \theta_\pi^{c.m.} < 1$ .  
 144 There is no distinct peak structure in the cross sections. The cross sections increase rapidly

145 when the  $\pi^-$  angle becomes smaller. A strong forward peaking of the cross sections is ob-  
 146 served. Similar strong forward peaking at  $|t| < 0.2 \text{ GeV}^2$  was reported for  $E_\gamma = 5, 8, 11,$  and  
 147  $16 \text{ GeV}$  by SLAC [14]. The momentum transfer of  $|t| < 0.2 \text{ GeV}^2$  corresponds to the  $\pi^-$   
 148 angular region of  $0.9 < \cos \theta_\pi^{c.m.} < 1$  in the present experiment. The exchange of an isospin  
 149  $I = 1$  meson ( $\pi$  or  $\rho$ ) in the  $t$  channel is expected to be the dominant reaction mechanism  
 150 in the present kinematical region. Since the  $\rho$ -meson exchange contribution becomes weak  
 151 at forward  $\pi$  angles in pion photoproduction [21],  $\pi$ -meson exchange is inferred to play an  
 152 important role in making the forward-peaking  $\pi^- \Delta^{++}$  cross sections for  $0.9 < \cos \theta_\pi^{c.m.} < 1$ .



153

154 FIG. 2. Differential cross sections for the  $\gamma p \rightarrow \pi^- \Delta^{++}$  reaction as a function of  $E_\gamma$ . The closed  
 155 circles, open circles, open triangles, open squares, and closed squares are the data obtained by  
 156 LEPS, SAPHIR [20], DESY [19], LAMP2 [18], and SLAC [16], respectively. Since the data obtained  
 157 by the other groups had the form  $d\sigma/dt$ , they were transformed to the form  $d\sigma/d \cos \theta_\pi^{c.m.}$  for the  
 158 comparison. The hatched histograms are the systematic uncertainties due to the selection of the  
 159  $\Delta^{++}$  shape. The solid curves are the results of theoretical calculations by S. i. Nam [28].

160 The LEPS cross sections for the  $\pi^- \Delta^{++}$  reaction are in good agreement with the cross  
 161 sections measured by DESY [19] and SLAC [16] overall. The LEPS cross sections also agree  
 162 well with those measured by LAMP2 [18] except for  $0.966 < \cos \theta_\pi^{c.m.} < 1$ . The cross sections  
 163 by SAPHIR [20] agree with the LEPS data for  $0.7 < \cos \theta_\pi^{c.m.} < 0.933$  and are smaller than



164 the LEPS data for  $0.933 < \cos \theta_{\pi}^{c.m.} < 0.966$ . Since the  $\pi^{-}\Delta^{++}$  reaction has strong forward-  
 165 peaking cross sections, small differences in the  $\pi^{-}$  angular regions between the SAPHIR and  
 166 present data might cause these disagreements.

167 Theoretical calculations, employing the tree-level Regge-Born interpolation model with-  
 168 out nucleon resonance contributions by S. i. Nam [28], almost reproduce the present cross  
 169 sections. Although the cutoff mass parameter was optimized from 450 MeV to 500 MeV to  
 170 fit the data, the energy dependence of the cross sections for  $0.9 < \cos \theta_{\pi}^{c.m.} < 1$  and  $E_{\gamma}=1.5$ -  
 171 1.8 GeV was not reproduced. One of the possible explanations for this discrepancy can be  
 172 attributed to the absence of resonance contributions in the theory. For instance,  $N^{*}(1900,$   
 173  $3/2^{+})$ , which strongly couples to  $\pi\Delta$ , could be responsible for describing a bump observed  
 174 in the cross section data. Since the  $s$ -channel structures observed in the SAPHIR total cross  
 175 sections [20] seem to continue up to  $E_{\gamma} \sim 2$  GeV, the excess in the present cross sections  
 176 might be the tail of  $s$ -channel structures.

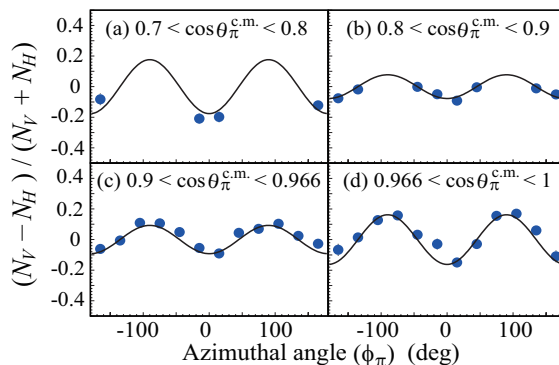
177 In this analysis, the relativistic Breit-Wigner form in Eq. (1) used by SLAC [14] was em-  
 178 ployed. Another analysis with a different relativistic Breit-Wigner shape used by DESY [19]  
 179 gave smaller cross sections than the present cross sections. The differences between the cross  
 180 sections obtained by the two Breit-Wigner forms are 10% on average and are shown in Fig. 2  
 181 as the largest systematic uncertainties. Since both of the relativistic Breit-Wigner shapes  
 182 originated from the shapes studied by Jackson [26], the differences in shape are not so large.  
 183 New analyses using different shapes for the  $\rho$ ,  $2\pi$ , and  $3\pi$  production events generated by  
 184 the simulations with different momentum and angular distributions were performed. The  
 185 differences between the original and new cross sections were smaller than 10% for most of  
 186 the data points. Systematic uncertainties of target thickness and photon flux are 1% and  
 187 3%, respectively.

188 The  $\vec{\gamma}p \rightarrow \pi^{-}\Delta^{++}$  reaction data were measured using vertically and horizontally polarized  
 189 photons. The photon-beam asymmetry  $\Sigma$  is given as

$$P_{\gamma}\Sigma \cos 2\phi_{\pi} = \frac{N_V - N_H}{N_V + N_H}, \quad (3)$$

190 where  $N_V$  and  $N_H$  are the  $\pi^{-}\Delta^{++}$  yields with vertically and horizontally polarized photons,  
 191 respectively, after correcting for the difference of photon flux in both polarizations.  $P_{\gamma}$  is the  
 192 polarization of the photons and  $\phi_{\pi}$  is the  $\pi^{-}$  azimuthal angle. The  $\pi^{-}\Delta^{++}$  yield is obtained  
 193 by fitting a missing-mass spectrum for each  $\phi_{\pi}$ ,  $\cos \theta_{\pi}^{c.m.}$ , and  $E_{\gamma}$  region. Figure 3 shows the

194 ratio  $(N_V - N_H)/(N_V + N_H)$  for the  $\pi^- \Delta^{++}$  reaction events for  $E_\gamma=1.5-2.9$  GeV.



195

196 FIG. 3. The ratio  $(N_V - N_H)/(N_V + N_H)$  as a function of  $\pi^-$  azimuthal angle ( $\phi_\pi$ ) for the  $\vec{\gamma}p \rightarrow$   
 197  $\pi^- \Delta^{++}$  reaction for  $E_\gamma=1.5-2.9$  GeV. The curves are the result of the fits with  $P_\gamma \Sigma \cos 2\phi_\pi$ .

198 Since the LEPS spectrometer has a wide acceptance for the horizontal direction and  
 199 a narrow acceptance for the vertical direction, the number of events is small at around  
 200  $\phi_\pi = \pm 90^\circ$  for  $0.7 < \cos \theta_\pi^{c.m.} < 0.9$ . The ratio  $(N_V - N_H)/(N_V + N_H)$  is large at  $\pm 90^\circ$  and is  
 201 small at  $0^\circ$  and  $180^\circ$ . The  $\pi^-$  mesons prefer to scatter at  $\phi_\pi$  angles parallel to the polarization  
 202 plane. The photon-beam asymmetries are therefore negative.

203 Figure 4 shows the photon-beam asymmetries for the  $\vec{\gamma}p \rightarrow \pi^- \Delta^{++}$  reaction. The system-  
 204 atic uncertainty of the laser polarization is  $\delta\Sigma=0.02$ . The effect of the electron contamination  
 205 in the  $\pi^-$  sample is removed and that of the start counter contamination in the LH<sub>2</sub> target  
 206 selection is negligibly small. The limited number of bins for the  $\pi^-$  azimuthal angle in Fig. 3  
 207 reduces absolute asymmetry values by 7% on average. The asymmetries obtained using a  
 208 different relativistic Breit-Wigner shape [19] agree with the present asymmetries. The dif-  
 209 ferences between the two asymmetries are  $\delta\Sigma=0.07$  on average and are shown in Fig. 4 as  
 210 the largest systematic uncertainties. New analyses using different shapes for the  $\rho$ ,  $2\pi$ , and  
 211  $3\pi$  production events generated by the simulations with different momentum and angular  
 212 distributions were performed. The differences between the original and new asymmetries  
 213 were smaller than the statistical errors. For the confirmation of the correctness of the asym-  
 214 metries, the sideband subtraction analysis using the sideband events of the  $\Delta^{++}$  peak was  
 215 performed, and the result of this analysis well reproduced the asymmetries in Fig. 4.

216 The asymmetries are found to be negative in most of the LEPS kinematical region,  
 217 which may be explained by  $\pi$ -meson exchange in the  $t$  channel. The same interpretation is

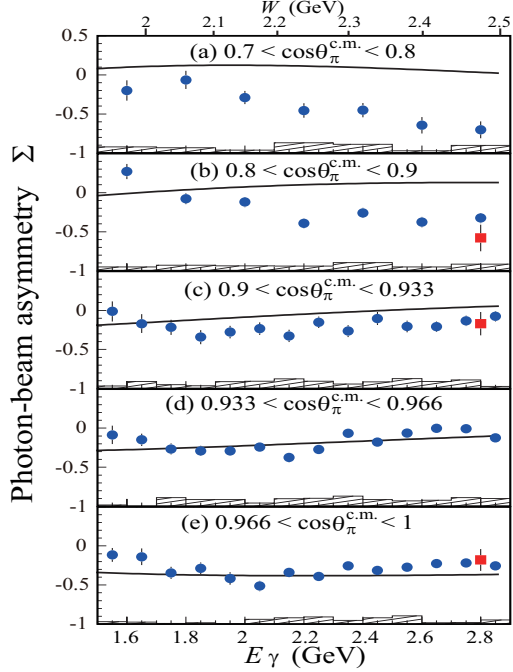


FIG. 4. Photon-beam asymmetries for the  $\vec{\gamma}p \rightarrow \pi^- \Delta^{++}$  reaction as a function of  $E_\gamma$ . The circles and squares are the data obtained by LEPS and SLAC [16], respectively. SLAC measured three asymmetries at  $|t|=0.2-0.5$ ,  $0.1-0.2$ , and  $|t_{min}|-0.1$  GeV<sup>2</sup>, and are plotted as squares in (b), (c), and (e). The hatched histograms are the systematic uncertainties due to the selection of the  $\Delta^{++}$  shape. The solid curves are the results of theoretical calculations by S. i. Nam [28].

218 obtained from the strong forward peaking of the cross sections observed in Fig 2. We have  
 219 observed positive asymmetries at forward pseudoscalar meson angles in most  $q\bar{q}$  productions  
 220 in the final state from the proton, such as a  $d\bar{d}$  production with  $\vec{\gamma}p \rightarrow \pi^+ n$  [1, 3] and an  $s\bar{s}$   
 221 production with  $\vec{\gamma}p \rightarrow K^+ \Lambda$  and  $K^+ \Sigma^0$  [4–8]. In addition, the photoproduction reactions  
 222 of neutral pseudoscalar mesons, such as  $\vec{\gamma}p \rightarrow \pi^0 p$  [3, 29] and  $\eta p$  [30, 31], also have positive  
 223 asymmetries at forward meson production angles. It is quite interesting that only pure  $u\bar{u}$   
 224 production in the final state has negative asymmetries. Since preliminary results of the  $\vec{\gamma}p$   
 225  $\rightarrow \pi^+ \Delta^0$  reaction show positive asymmetries [32], the production of the spin-parity  $3/2^+$   
 226 baryon does not necessarily cause the negative asymmetries.

227 SLAC measured three asymmetries at  $E_\gamma=2.8$  GeV [16]. The agreement between the  
 228 LEPS and SLAC data is reasonable for  $0.9 < \cos\theta_\pi^{c.m.} < 0.933$  and  $0.966 < \cos\theta_\pi^{c.m.} < 1$ . The  
 229 SLAC data for  $0.8 < \cos\theta_\pi^{c.m.} < 0.9$  is slightly smaller than for the LEPS data.

230 Since the asymmetry calculated in Ref. [28] has an opposite definition, it is corrected to

231 meet the present definition in Eq. (3). Theoretical calculations by S. i. Nam [28] almost  
 232 reproduce the negative asymmetry data for  $0.933 < \cos \theta_{\pi}^{c.m.} < 1$ . As the  $\pi$  angle becomes  
 233 larger, the calculations predict small positive asymmetries since the  $\pi$ -exchange contribution  
 234 becomes small. The inconsistency between the data and the calculations becomes large for  
 235  $0.7 < \cos \theta_{\pi}^{c.m.} < 0.9$ . This inconsistency is inferred to be due to the possible existence of a  
 236 small but finite additional unnatural-parity exchange contribution not taken into account  
 237 in the theory calculations. Smaller absolute asymmetry values at  $E_{\gamma}=1.5-1.7$  GeV and  
 238  $0.9 < \cos \theta_{\pi}^{c.m.} < 1$  might be caused by the bump observed in the cross sections (Fig. 2).

239 In summary, we have carried out a photoproduction experiment observing the  $\vec{\gamma}p \rightarrow$   
 240  $\pi^{-}\Delta^{++}$  reaction by using linearly polarized tagged photons with energies from 1.5 to 2.95  
 241 GeV. Differential cross sections and photon-beam asymmetries have been measured for  $0.7 <$   
 242  $\cos \theta_{\pi}^{c.m.} < 1$ . There is no distinct peak structure in the cross sections. However, a non-  
 243 negligible excess of the cross sections, possibly due to the tail of nucleon or  $\Delta$  resonances,  
 244 over the theoretical predictions is observed at  $E_{\gamma}=1.5-1.8$  GeV. Strong forward-peaking  
 245 cross sections, expected from  $\pi$  exchange in the  $t$  channel, are observed. The asymmetries  
 246 for the  $\pi^{-}\Delta^{++}$  reaction are found to be negative in most of the present kinematical regions,  
 247 which suggests that the  $\pi$  exchange in the  $t$  channel is dominant. The negative asymmetries  
 248 are unusual in the photoproduction reactions from the proton studied in the past [1, 3–  
 249 8]. Analogous results were obtained in the measurements of the single-spin asymmetries  
 250 for the  $pp$  or  $ep$  reactions [33], where inclusive  $\pi^{-}$  production has negative asymmetries  
 251 while inclusive  $\pi^{+}$  and  $K^{+}$  productions have positive asymmetries. The  $\pi^{-}$  production is  
 252 inferred to have a different reaction mechanism from the  $\pi^{+}$  and  $K^{+}$  productions. The  $\gamma p \rightarrow$   
 253  $\pi^{-}\Delta^{++}$  reaction data provide a unique chance for studying the  $u\bar{u}$  quark pair production.  
 254 The combination of these data with the established data for the  $d\bar{d}$  and  $s\bar{s}$  quark pair  
 255 productions is helpful to achieve unified understanding of the hadron photoproduction.

## 256 ACKNOWLEDGMENTS

257 The authors gratefully acknowledge the staff of the SPring-8 facility for the supports with  
 258 excellent experimental conditions. The experiments were performed at the BL33LEP of  
 259 SPring-8 with the approval of the Japan Synchrotron Radiation Research Institute (JASRI)  
 260 as a contract beamline (Proposal No. BL33LEP/6001). H.K. thanks Prof. E. Oset, Prof.

261 T. Mart, Prof. S. Kumano, and Prof. H. Kamano for fruitful discussions. This research  
262 was supported in part by the Ministry of Education, Science, Sports and Culture of Japan,  
263 the National Science Council of the Republic of China, the National Research Foundation  
264 of Korea, and the U.S. National Science Foundation.

---

- 265 [1] H. Kohri *et al.*, Phys. Rev. C **97**, 015205 (2018).
- 266 [2] M. Dugger *et al.*, Phys. Rev. C **79**, 065206 (2009).
- 267 [3] M. Dugger *et al.*, Phys. Rev. C **88**, 065203 (2013).
- 268 [4] M. Sumihama *et al.*, Phys. Rev. C **73**, 035214 (2006).
- 269 [5] H. Kohri *et al.*, Phys. Rev. Lett. **97**, 082003 (2006).
- 270 [6] A. Lleres *et al.*, Eur. Phys. J. A **31**, 79 (2007).
- 271 [7] C. A. Paterson *et al.*, Phys. Rev. C **93**, 065201 (2016).
- 272 [8] S. H. Shiu *et al.*, Phys. Rev. C **97**, 015208 (2018).
- 273 [9] R. Bradford *et al.*, Phys. Rev. C **73**, 035202 (2006).
- 274 [10] M. E. McCracken *et al.*, Phys. Rev. C **81**, 025201 (2010).
- 275 [11] B. Dey *et al.*, Phys. Rev. C **82**, 025202 (2010).
- 276 [12] S. Capstick and W. Roberts, Phys. Rev. D **49**, 4570 (1994).
- 277 [13] R. L. Anderson *et al.*, Phys. Rev. D **14**, 679 (1976).
- 278 [14] A. M. Boyarski *et al.*, Phys. Rev. Lett. **22**, 148 (1969).
- 279 [15] A. M. Boyarski *et al.*, Phys. Rev. Lett. **25**, 695 (1970).
- 280 [16] J. Ballam *et al.*, Phys. Rev. D **5**, 545 (1972).
- 281 [17] Cambridge Bubble Chamber Group, Phys. Rev. **163**, 1510 (1967).
- 282 [18] D. P. Barber *et al.*, Z. Phys. C **6**, 93 (1980).
- 283 [19] ABBHHM Collaboration, Phys. Rev. **175**, 1669 (1968).
- 284 [20] C. Wu *et al.*, Eur. Phys. J. A **23**, 317 (2005).
- 285 [21] M. Guidal, J.-M. Laget, M. Vanderhaeghen, Phys. Lett. B **400**, 6 (1997).
- 286 [22] D.J. Quinn *et al.*, Phys. Rev. D **20**, 1553 (1979).
- 287 [23] T. Nakano *et al.*, Nucl. Phys. A **684**, 71 (2001).
- 288 [24] N. Muramatsu *et al.*, Nucl. Instr. Meth. A **737**, 184 (2014).
- 289 [25] S. H. Hwang, Ph.D. thesis, Pusan National University, 2012 (unpublished).

- 290 [26] J. D. Jackson, *Nuovo Cimento* **34**, 1644 (1964).
- 291 [27] G. Boschhorn *et al.*, *Phys. Rev. Lett.* **18**, 571 (1967).
- 292 [28] Seung-il Nam and Byung-Geel Yu, *Phys. Rev. C* **84**, 025203 (2011).
- 293 [29] N. Sparks *et al.*, *Phys. Rev. C* **81**, 065210 (2010).
- 294 [30] D. Elsner *et al.*, *Eur. Phys. J. A* **33**, 147 (2007).
- 295 [31] P. Collins *et al.*, *Phys. Lett. B* **771**, 213 (2017).
- 296 [32] H. Kohri, *JPS Conf. Proc.* **10**, 010008 (2016).
- 297 [33] C. A. Aidala *et al.*, *Rev. Mod. Phys.* **85**, 655 (2013).